nature chemistry

ARTICLES

PUBLISHED ONLINE: 13 FEBRUARY 2017 | DOI: 10.1038/NCHEM.2720

Tuning underwater adhesion with cation–π interactions

Matthew A. Gebbie[1,2], Wei Wei[2], Alex M. Schrader[2,3], Thomas R. Cristiani[1], Howard A. Dobbs[4], Matthew Idso[4], Bradley F. Chmelka[4], J. Herbert Waite[2,3]* and Jacob N. Israelachvili[1,2,4]*

Cation–π interactions drive the self-assembly and cohesion of many biological molecules, including the adhesion proteins of several marine organisms. Although the origin of cation–π bonds in isolated pairs has been extensively studied, the energetics of cation–π-driven self-assembly in molecular films remains uncharted. Here we use nanoscale force measurements in combination with solid-state NMR spectroscopy to show that the cohesive properties of simple aromatic- and lysine-rich peptides rival those of the strong reversible intermolecular cohesion exhibited by adhesion proteins of marine mussel. In particular, we show that peptides incorporating the amino acid phenylalanine, a functional group that is conspicuously sparing in the sequences of mussel proteins, exhibit reversible adhesion interactions significantly exceeding that of analogous mussel-mimetic peptides. More broadly, we demonstrate that interfacial confinement fundamentally alters the energetics of cation–π-mediated assembly: an insight that should prove relevant for diverse areas, which range from rationalizing biological assembly to engineering peptide-based biomaterials.

Nature employs a variety of non-covalent interactions to tune the structures and functions of proteins, peptides and other complex biological molecules with cation–π interactions that feature prominently in biological self-assembly[1–4], molecular recognition[5–7] and molecular cohesion and adhesion[8–10]. In composite materials, such as protein–solid interfaces, delamination can occur within a glue (peptide) film, which is called cohesive failure. Delamination can also occur at a glue–surface (peptide-surface) interface, which is called adhesive failure (Supplementary Fig. 1). These two terms are often used interchangeably in the broader scientific literature, and many adhesives actually fail via cohesive mechanisms[11–13].

Cation–π interactions are electrostatic in origin and occur between cations and electron-rich π orbitals[1,14,15]. Particularly strong cation–π binding occurs when cations interact with the delocalized π orbitals perpendicular to the plane of aromatic rings. Although cation–π interactions are much stronger in the gas phase than in condensed phases, they still exceed the strength of hydrogen bonds, and possibly even charge–charge interactions, in aqueous solutions[1,16]. As a result, cation–π interactions provide an attractive molecular design model to develop molecules that can function as adhesives in underwater environments. Such materials could be used to address a number of substantial engineering challenges, which range from functioning as biomedical adhesives that can replace damaging screws in surgical applications[17] to providing cohesive binding domains that hold together tissue-engineering scaffolds[18].

Despite this technological promise, the relative binding energetics of cation–π interactions at interfaces cannot yet be predicted *a priori*. Indeed, much of the current understanding of cation–π binding strengths in condensed phases is either extrapolated from gas-phase experiments and calculations[1,14–16] or inferred from the proximity of aromatic and cationic amino acids in protein crystal structures[2,3,6]. Nevertheless, it remains unclear whether these insights are directly applicable to rationalizing cation–π energetics at interfaces.

Notably, cation–π binding at interfaces typically involves the formation of several cation–π binding pairs in close proximity, in which the electrostatic repulsion between two closely spaced (positive) pairs can compromise the favourable free energy gained by forming the two cation–π bonds. The complexation of anions with cation–π pairs could provide the necessary charge compensation to eliminate this electrostatic repulsion. Indeed, researchers have studied the impact of anions on isolated ternary cation–π–anion binding groups[19–23], but emphasized that the three-body interaction term in cation–π–anion complexation is anti-cooperative and weakens the interaction strength of (destabilizing) cation–π binding pairs. However, these previous studies did not account for the electrostatic repulsion between closely spaced cation–π binding groups, which we hypothesize is an important general effect at interfaces and in the interiors of folded proteins. As a result, to gain insight into the impact of electrostatic correlations between cation–π binding pairs on the energetics of cation–π interactions is of practical relevance.

In the context of engineered biomaterials, cation- and aromatic-rich sequences are prevalent in the adhesive proteins of several marine organisms, including mussels[17], sandcastle worms[24] and barnacles[25]. Many researchers have sought to translate these protein sequences into synthetic, bioinspired adhesives by focusing predominantly on the role of the catecholic functional group 3,4-dihydroxyphenylalanine (Dopa)[17,26–30]. However, these same studies[26,28,30] indicate that a reliance on Dopa alone is unrealistic for engineering an effective wet adhesion in underwater environments. Further, Dopa is conspicuously sparing or non-existent in the highly adhesive proteins of some marine organisms, such as green mussels[8] and barnacles[25], whereas Dopa is prevalent in non-adhesive proteins, such as the plaque-coating proteins of some marine mussels[17]. More recent studies[31,32] identified a possible synergistic relationship between Dopa and cationic amino acids; yet none of these studies systematically explored how changes to the

[1]Materials Department, University of California, Santa Barbara, California 93106, USA. [2]Materials Research Laboratory, University of California, Santa Barbara, California 93106, USA. [3]Department of Molecular, Cell and Developmental Biology, University of California, Santa Barbara, California 93106, USA. [4]Department of Chemical Engineering, University of California, Santa Barbara, California 93106, USA.
*e-mail: jacob@engineering.ucsb.edu; waite@lifesci.ucsb.edu

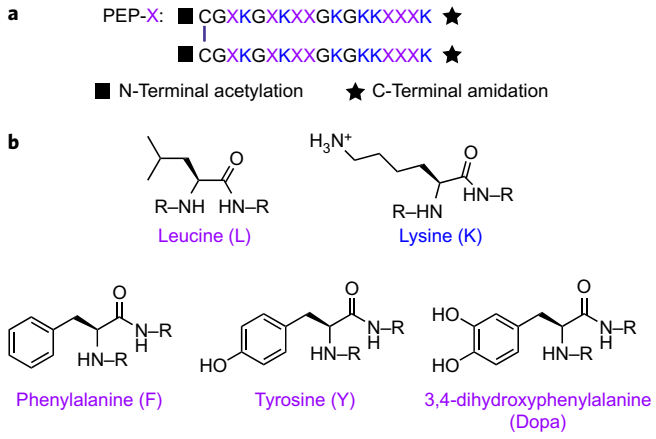

Figure 1 | Sequences and molecular structures of the peptides studied. **a**,**b**, Each of the four peptides included one of the amino acids illustrated in **b**, incorporated in the sequence locations marked by a purple 'X' in **a**. The Lys residues are conserved in each peptide sequence and are marked in blue to emphasize the positive charge of Lys at a pH of 2.5.

aromatic molecular structure impact the strength of cation–π interactions in adhesive films.

In this work, we test the hypothesis that cation–π interactions may provide a broader molecular motif that can be used to imbue peptide-based materials with robust underwater cohesion and pursue fundamental insights into the energetics of interfacial cation–π interactions. To test this proposal, we designed a series of lysine- and aromatic-rich peptides and used nanoscale force measurements to determine quantitatively the cohesion-interaction strength present within films composed of each peptide.

Results

Peptide design. All four of the peptides are composed of a sequence of 36 amino acids, with the numbers and locations of the glycine (Gly), lysine (Lys) and cysteine (Cys) residues conserved (Fig. 1). The locations of the aromatic residues and leucine (Leu) hydrophobic control (X) were also conserved. The four peptides differ only by progressive hydroxylation of the aromatic residue in three of the peptides: phenylalanine (Phe), tyrosine (Tyr) and 3,4-dihydroxyphenylalanine (Dopa). The fourth peptide is a Leu analogue to test whether the strong adhesion forces we measure result from nonspecific hydrophobic and/or hydrogen-bonding interactions.

The overall sequence is inspired by a Lys- and Dopa-rich sequence of 16 amino acids that is present in the mussel foot protein mefp-5, a strongly adhesive mussel foot protein prominently featured at the mussel adhesive plaque-solid interface[31,33]. Dopa is also the dominant aromatic residue in many mussel foot proteins, and thus we refer to the Dopa peptide as a mussel-mimetic peptide sequence. Although some mussel proteins also contain an appreciable Tyr content, Phe is conspicuously deficient in marine mussel adhesive proteins.

Mica was selected as the substrate material because primary amines, like Lys, strongly bind to the surface of mica via ion exchange with the K^+ ions present at the surface of single-crystalline mica[9,34]. Although individual Lys–mica Coulomb bonds are weaker than covalent interactions, the peptides form multiple Lys–mica bonds with an energy of between 3 and 5 k_BT each. The peptides irreversibly adsorb to mica under the conditions tested, so the adhesion forces across the confined peptide films are proportional to the cohesion interactions between peptide molecules.

Analysis of force–distance profiles. When mica surfaces are approached and separated in the background buffer solution (no peptide) of 100 mM acetic acid and 250 mM KNO_3 (hereafter 'high salt conditions') using the surface forces apparatus (SFA)[35] (Fig. 2), the forces are reversibly repulsive on both approach and separation (Fig. 3). The surface separation distance, D, is defined with respect to the hard contact of two mica surfaces in an inert nitrogen atmosphere, where $D = 0$ nm. The non-monotonic features measured for surface separation distances, D, of less than 2 nm are consistent with other measurements across highly concentrated electrolyte solutions and result from the ordering and/or correlation of ions between the mica surfaces.

Although the focus of this work is on the adhesion forces of peptides in high salt conditions, force–distance curves were also measured for the Tyr and Phe peptides in 100 mM acetic acid solutions with variable concentrations of KNO_3. These experiments are presented in Supplementary Figs 3 and 4 and demonstrate that cohesion forces systematically decrease as the background solution salinity is increased. These experiments illustrate that the deposition salinity may need to be matched to the salinity present in the application to enable the maximum adhesion performance.

All four of the peptides form diffusive, hydrated surface films that are approximately 3–5 nm in thickness when solution deposited onto a single mica surface under high salt conditions (Fig. 3). The (positive) repulsive forces that are measured when bringing peptide-coated surfaces together originate from compressing the diffusive films into tightly packed configurations (Fig. 2). The ranges of these repulsive forces differ by 3–4 nm among different experiments. As discussed in Methods, unavoidable changes in the optical path occur when the surfaces are removed from the SFA to deposit peptides after calibrating the mica thickness, which results in up to a 2 nm uncertainty in the peptide-film thicknesses. Critically, the magnitudes of the repulsive forces and the distances over which one can compress the films is characteristic of the peptide molecular structure and solution salinity, and remains independent of variability in the measured film thickness. During compression, the slope of the force–distance profile is roughly proportional to the compressibility of the peptide films, so we conclude that the three aromatic peptide films exhibit similar mechanical properties during compression; the Leu peptide formed less-compressible films.

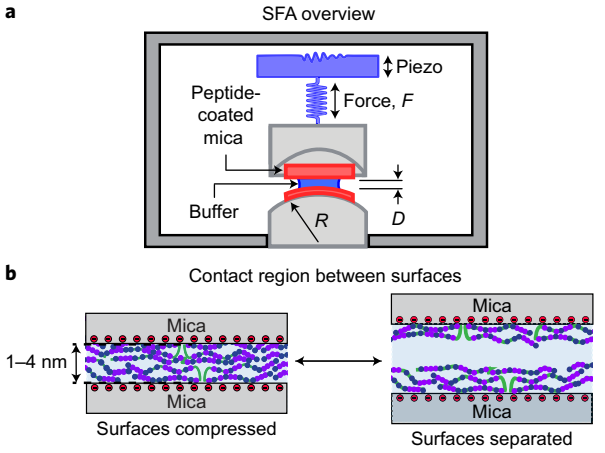

Figure 2 | Schematic of the SFA set-up and illustration of the surface–peptide–surface interface studied. a, SFA experimental set-up. The peptide was solution deposited onto mica surfaces before placing it into the SFA, and all the experiments were performed in a pH 2.5 buffer solution of 100 mM acetic acid and 250 mM KNO_3, without additional dissolved peptide. **b**, When the two surfaces are compressed into hard contact, a multilayer peptide film is confined between the two surfaces. When the surfaces are separated, failure occurs within the peptide film, which means that the measured work of adhesion is proportional to the intermolecular interactions between peptide molecules.

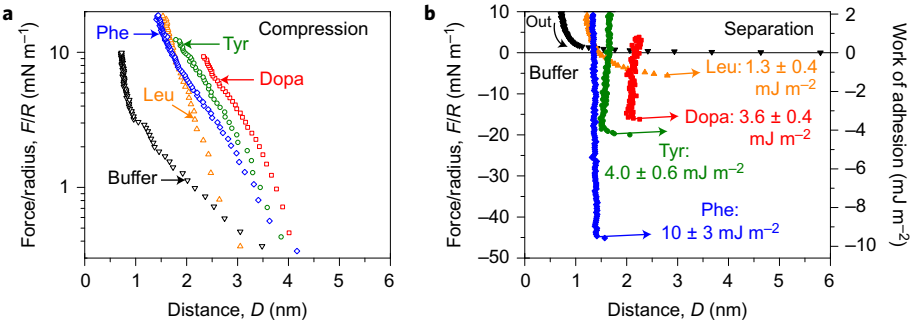

Figure 3 | Representative force–distance data measured for peptides between mica surfaces. a, Representative force–distance profiles measured when two mica surfaces are brought together in 100 mM acetic acid and 250 mM KNO_3. Measurements were also performed under variable solution salinities and are presented in Supplementary Figs 4 and 5. Positive forces are repulsive and negative forces are attractive. The black data were measured in the absence of adsorbed peptide, and each of the coloured curves corresponds to an experiment in which the peptide was adsorbed onto a single mica surface. **b**, Representative profiles measured when mica surfaces are separated in 100 mM acetic acid and 250 mM KNO_3. The black force–distance profile measured in the absence of peptide exhibits repulsive behaviour, which supports that the adhesion measured in the presence of peptide films results from peptide intermolecular cohesion. The average work of adhesion and associated uncertainty quoted on the plot was obtained from at least ten different force–distance profiles for each peptide. Small variations in peptide-film thicknesses were measured between different experiments, and these variations exhibited no dependence on the peptide molecular structure. Importantly, the work of adhesion does not exhibit a systematic dependence on the film thickness, which implies that the cohesion interactions are independent of minor variations in the film thickness.

In contrast, the adhesion forces that are measured when separating the mica surfaces exhibit a significant dependence on the peptide molecular structure (Fig. 3). For the Leu peptide (hydrophobic control) at high salt conditions, the work of adhesion was measured as 1.3 ± 0.4 mJ m^{-2} and the attractive force extended over a distance of 1–2 nm. The range and magnitude of this force is consistent with the pulling apart of weak, nonspecific cohesion interactions that probably result from hydrophobic interactions and intermolecular hydrogen bonding along the peptide backbones.

All three aromatic peptides exhibit dramatically increased adhesion relative to the Leu control (Fig. 3). As a pronounced strong adhesion is measured only when the peptides contain both cationic (Lys) and aromatic moieties, and this adhesion is strongly impacted by changing the solution salinity, we conclude that the most-probable source of the strong adhesion measured in the three aromatic peptides is intermolecular cation–π interaction. Solid-state NMR spectroscopy corroborates this conclusion, as discussed below.

The work of adhesion measured for the mussel-mimetic Dopa peptide, 3.6 ± 0.4 mJ m^{-2}, and for the Tyr peptide, 4.0 ± 0.6 mJ m^{-2}, are similar, with the Tyr peptide yielding a work of adhesion that slightly exceeds that of the mussel-mimetic Dopa peptide. This observation indicates that the interfacial Lys–Tyr and Lys–Dopa cation–π complexation energies are similar. This result also implies that the cation–π interaction between Dopa and Lys is the dominant mechanism that mediates molecular cohesion in Dopa- and Lys-containing proteins, peptides and synthetic molecules.

Unexpectedly, the measured work of adhesion for the Phe peptide is 10 ± 3 mJ m^{-2}, which is more than double that measured for the Tyr and Dopa peptides. From this result, we conclude that the Phe–Lys cation–π complexation energy is surprisingly strong compared with the Tyr–Lys and Dopa–Lys complexation energies.

Solid-state NMR spectroscopy. Solid-state NMR spectroscopy complements the SFA measurements by establishing the molecular proximities and orientations of lysine and aromatic residues in solid (non-crystalline) peptides as a model of the intermolecular interactions that occur in peptide-rich confined films. Two-dimensional (2D) $^{13}C\{^1H\}$ heteronuclear correlation (HETCOR) experiments use through-space dipolar couplings to correlate the isotropic chemical shifts of nearby (<1 nm) ^1H and ^{13}C nuclei. The solid-state 2D $^{13}C\{^1H\}$ HETCOR spectrum of Tyr in Fig. 4 shows many well-resolved correlations that arise from dipolar-coupled ^{13}C and ^1H nuclei of the Tyr peptide. Most intensity correlations in this 2D spectrum originate from directly bound intraresidue ^1H and ^{13}C nuclei, which allows their assignments to specific ^1H and ^{13}C moieties of the lysine, tyrosine, cysteine and glycine residues of the Tyr peptide. These resonance assignments are corroborated by the solid- and solution-state NMR spectra of neat peptides and polypeptides reported in the literature[36–40].

Importantly, the 2D $^{13}C\{^1H\}$ HETCOR spectrum (Fig. 4) of Tyr also includes intensity correlations that result from inter-residue interactions, specifically among the lysine and tyrosine side chains. In particular, ^1H signals at ~6.6 ppm of the aromatic ^1H moieties of the tyrosine residues are correlated with ^{13}C signals between 20 and 30 ppm (Fig. 4, red arrows) assigned to the alkyl l and m moieties of the lysine residues. These correlations unambiguously establish the close proximities of the alkyl groups of lysine with the aromatic tyrosine moieties.

Furthermore, the ^{13}C signals at ~40 ppm (Fig. 4, red shaded region) from the alkyl j^+ moieties are correlated with ^1H signals at 6.9 ppm of the ε^+ ^1H moieties of the protonated lysine amide groups. By comparison, a 2D $^{13}C\{^1H\}$ HETCOR spectrum (Supplementary Fig. 5) collected from the Leu peptide without aromatic residues under otherwise identical conditions shows that the intensity correlation from the same j^+ ^{13}C and ε^+ ^1H moieties occurs at ~7.5 ppm in the ^1H dimension. The large displacement (0.6 ppm) of this correlated intensity to a lower frequency in the spectrum of the Tyr peptide (Fig. 4) indicates that the ε^+ ^1H groups experience ring-current effects that are associated with a substantial fraction of these ^1H moieties positioned near the centres of the aromatic rings of the tyrosine side chains, as shown schematically in Fig. 4. Such a configuration of the tyrosine and lysine side chains is consistent with cation–π interactions among the protonated lysine and tyrosine side chains and corroborates the analyses of the SFA data.

Discussion

The adhesion forces that we measured for all three aromatic- and Lys-containing peptides are consistent with the work of adhesion measured previously for various Dopa-containing mussel adhesive proteins between mica surfaces, under similar conditions of salinity and pH (ref. 17). Surprisingly, the Phe peptide exhibits an adhesive performance between mica surfaces that exceeds the performance of the mussel-mimetic Dopa peptide and even rivals that of the

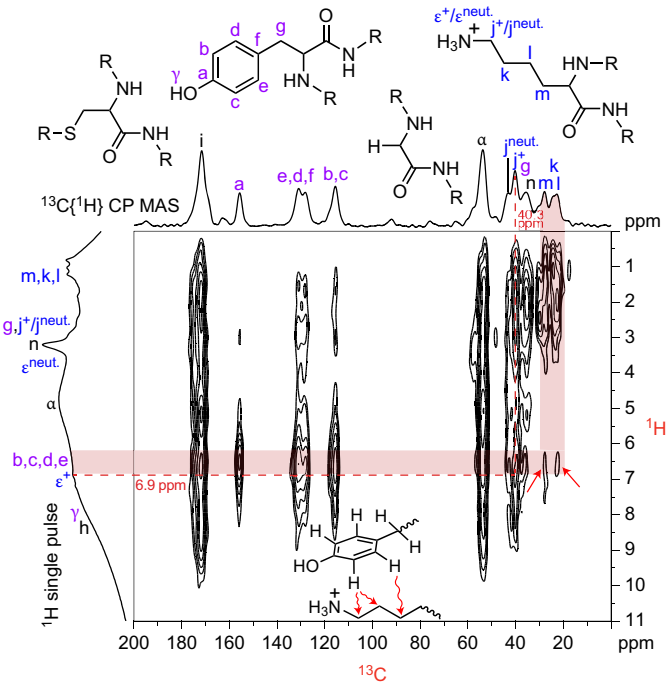

Figure 4 | Solid-state 2D ^{13}C{^{1}H} HETCOR MAS NMR spectrum acquired from bulk Tyr peptide with a 1D ^{13}C{^{1}H} CP MAS NMR spectrum along the top horizontal axis and a single-pulse ^{1}H MAS NMR spectrum along the left vertical axis. Red arrows indicate the intensity correlations that result from the close proximities (<1 nm) of the aromatic b–e ^{1}H moieties of the tyrosine residues (purple letters) and alkyl l and m ^{13}C moieties of the lysine side chains (blue letters). The superscript '+' denotes chemical shifts associated with protonated (positive) lysine residues, whereas the superscript 'neut.' denotes chemical shifts associated with neutral lysine residues. The intersection of the shaded red bands indicates a correlated intensity that arises from the proximate alkyl j ^{13}C moieties and protonated amide ε^{+} ^{1}H moieties of lysine residues, which resonate approximately 0.6 ppm to a lower frequency in the ^{1}H dimension compared with a Leu sample measured under otherwise identical conditions (Supplementary Fig. 5). Such a displacement is consistent with ring-current effects that would result from a configuration of the lysine and tyrosine side chains shown schematically in the inset, associated with inter-residue contact through cation–π electron interactions. All the NMR measurements were conducted at 11.74 T under 10 kHz MAS conditions at 0 °C.

most-adhesive Dopa-containing mussel foot protein tested to date, mefp-5 (ref. 33)

Nevertheless, Dopa is a biologically important functional group that exhibits diverse chemical reactivity[17]. For example, Dopa can chelate multivalent ions[41,42] and exhibits a propensity to autoxidize and irreversibly crosslink at neutral-to-basic pH conditions[43,44]. Certainly, this reactivity can be used to advantage. Unfortunately, in many circumstances the oxidation state of Dopa cannot be controlled easily[43–45], which leaves the adhesive properties of Dopa-containing molecules compromised by premature autoxidation. Our results suggest that molecules incorporating Lys and a balance of both Dopa and chemically stable Phe could provide an attractive alternative for developing underwater adhesives, hydrogel binding groups and other applications that involve molecular cohesion in harsh oxidizing environments.

Our results also provide additional evidence to support the importance of cation–π interactions in marine bioadhesion. Many mussel proteins comprise sequences that are rich in both Lys and Dopa residues[17]. Recently, the adhesion of synthetic biomimetic small-molecule monolayers to mica surfaces was shown to depend critically on the synergy between Dopa and Lys functional groups[32], with the conclusion that the primary role of Lys is to eject hydrated cations from mica surfaces to enable Dopa-surface bidentate hydrogen bonding. This prior study[32] proposed that an analogous effect occurs in the larger adhesion proteins utilized by marine mussels. This interpretation predicts that surface-binding interactions between Dopa-containing peptides and mica surfaces should significantly exceed those in Tyr- or Phe-based peptides, whereas we observed similar adhesion forces for the Dopa and Tyr peptides, and increased adhesion in the Phe peptide.

We rationalize this observation by noting that Maier *et al.*[32] studied monolayers of a small molecule, for which adhesive failure necessarily occurs at the molecule–mica interface. Here, the failure plane is shifted out into the peptide film, which results in cohesive failure, as is the case for most practical adhesives composed of larger molecules, such as peptides and proteins, that assemble to encapsulate particles and/or cover surface heterogeneities[11–13,46]. For large molecule multilayers that strongly bind to surfaces through multiple parallel covalent bonds, hydrogen bonds and/or strong ionic bonds, molecule–molecule interactions are often weaker (and/or more transient) than molecule–surface interactions. This shifts failure planes away from surfaces and into the films[13], which renderers the overall adhesive performance critically dependent on intermolecular cohesion.

Thus, the molecule–surface binding force and/or energy of the mussel-mimetic Dopa peptide may exceed the surface binding of the Phe peptide; this does not contradict the observation that the cation–π-mediated cohesion in Phe significantly exceeds that of Dopa. Furthermore, these results can be explained without invoking bidentate Dopa hydrogen bonding because a combination of Lys electrostatic interactions and/or peptide-backbone hydrogen bonds appear to be sufficient for strong peptide–surface binding. Nevertheless, prior evidence[31,32,44,47] indicates that bidentate hydrogen bonding should be important whenever the film-failure plane is located at the molecule–surface interface, especially in the absence of Lys residues.

With this in mind, we address the sometimes contradictory conclusions as to the importance of Dopa bidentate hydrogen bonding for promoting underwater adhesion. Specifically, several groups (including ours)[31–33] previously concluded that Dopa-mediated bidentate hydrogen bonding is critical to enable mussel proteins to achieve a strong underwater adhesion. Many of these studies controlled for the role of hydrogen bonding by chemically oxidizing Dopa to dopaquinone, which demonstrated a corresponding decrease in adhesion. However, dopaquinone is a reactive functional group that can induce a wide range of chemical and/or conformational changes within protein and peptides[17]. Thus, oxidizing Dopa to dopaquinone does much more than remove the opportunity for bidentate hydrogen bonding.

Recently, there have been efforts[10,31] to compare the adhesion of mussel-mimetic peptides and recombinant proteins that incorporate Tyr in peptides analogous to the Dopa peptides to test the impact of bidentate hydrogen bonding. Peptide adhesion was observed to be similar for the Dopa and Tyr functionalities in peptides that contained significant numbers of cationic residues[10], in agreement with the current study. In contrast, underwater adhesion was seen to depend on the presence of bidentate Dopa hydrogen binding in peptides that lacked cationic residues[31]. Notably, the adhesion of non-cationic sequences was observed to be significantly lower than that measured for positive (cationic) peptides that are rich in aromatic groups[31].

Further, many prior studies did not focus on establishing whether films fail through adhesive or cohesive mechanisms, which leaves open the possibility that film-failure mechanisms may also play a large role in determining the importance of bidentate hydrogen bonding. For example, bidentate hydrogen bonding

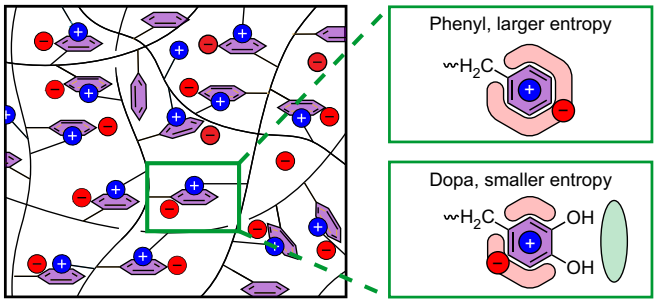

Figure 5 | Schematic that depicts the proposed mechanism of cation–π binding in aromatic- and Lys-rich peptide films, with many cation–aromatic binding pairs forming in close proximity. Each cation–π pair is positively charged, and anion complexation is required to avoid strongly repulsive electrostatic interactions. The most favourable configuration for the anions is within the plane of the aromatic rings, as illustrated by the shaded pink areas that surround the aromatic groups. Aromatic hydroxylation reduces the total volume of favourable anion-interaction sites that are in direct molecular contact with the aromatic ring, illustrated by the reduced pink area in the Dopa panel relative to the Phe panel. Aromatic hydroxylation may also provide a second type of anion interaction site that could be important for anions that form strong hydrogen bonds, illustrated by the green area. The potential importance of hydrogen bonding between ions and aromatic substituents awaits future studies. We propose that an increased configurational entropy within the Phe films is the molecular origin of the increased cohesion present in the Phe peptide relative to the Dopa and Tyr peptides.

interactions may ultimately be crucial for most films in which failure occurs at the molecule–surface interface, as has been shown for small-molecule adhesives[32] and catechol-functionalized self-assembled monolayers[47]. We further address the issue of distinguishing between failure modes in the Establishing Cohesive Failure section of the Supplementary Information.

Given this information, we propose that the adhesion synergy previously observed in Dopa- and Lys-rich mussel foot proteins, in which cohesion often plays a critical role, may primarily be attributed to cation–π interactions, as opposed to surface hydrogen-bonding interactions. Further, our results provide a molecular basis for understanding how the aromatic- and cation-rich proteins produced by organisms that do not leverage the Dopa functional group, such as barnacles[25], can presumably achieve molecular cohesion rivalling that of Dopa-rich mussel foot proteins.

More broadly, our work demonstrates that the physical chemistry of cation–π complexation in confinement substantially differs from the predictions of gas-phase calculations. For example, quantum chemical calculations of cation–aromatic binding pairs show that the interaction energies of K^+–benzene and K^+–phenol interactions agree to within fractions of 1 k_BT (ref. 1) because of the counterbalancing σ-withdrawing and π-donating effects exerted by hydroxyl groups on the electron density of aromatic rings. By this reasoning, the subsequent hydroxylation of phenol should minimally impact the energetics of cation–π binding, and the cation–π binding energies of the Phe, Tyr and Dopa peptides should be similar.

Instead, we find that the peptide adhesion strength exhibits a pronounced dependence on the presence of aromatic-ring hydroxylation, with the Phe peptide exhibiting intermolecular cohesion that is more than double that of either the Tyr or Dopa peptides. This observation cannot be explained via calculations of binary cation–aromatic binding energies, but is consistent with a previous study of cation–π interactions in self-assembled monolayers[9], in which the interaction energy between poly-L-Lys films and polystyrene films was measured to be about twice as strong as that between poly-L-Lys films and poly-L-Tyr films. This study did not comment on the possible molecular origins of this observation.

To explain both our results and these previous[9] results, we propose that anion complexation with the positive cation–π binding pairs is necessary to form stable cation–π bonds in confined interfaces (Fig. 5). In the absence of anions, the cation–aromatic binding pairs within the peptide film would repel electrostatically. Hence, the peptide films must contain enough anions to neutralize most of the cation–aromatic binding pairs. Calculations on cation–π–anion complexation[21–23] show that anions interact strongly with the cation as well as with the polarized hydrogens in the plane of the aromatic rings.

For entropic reasons, complexed anions are expected to be delocalized within the peptide films, as depicted in Fig. 5, as opposed to being located in static configurations. We propose that the presence of bulky electronegative hydroxyl substituents decreases the total number of favourable anion interaction sites, which leads to a corresponding decrease in the configurational entropy of the peptide films (Fig. 5). Hence, we deduce that an increased configurational entropy within the Phe films is the molecular origin of the increased cohesion exhibited by the Phe peptide relative to the Dopa and Tyr peptides.

We conclude further that to replace even a single aromatic-ring hydrogen with a bulky electronegative hydroxyl group abruptly decreases the strength of the cation–π-mediated cohesion within the peptide films, whereas the addition of a second hydroxyl group leads to only a marginal additional decrease in the peptide cohesion. Thus, we demonstrate that the rational inclusion or exclusion of aromatic-ring hydroxyl groups in peptide-binding domains provides a facile molecular strategy for tuning the cohesion-binding strength of cation–π interactions.

Conclusion

We established that that the cohesion of short aromatic- and Lys-rich peptides rivals the strong reversible intermolecular cohesion exhibited by full mussel adhesive proteins. Thus, these engineered short peptides self-assemble to form nanoscale films that mediate reversible underwater adhesion between solid surfaces rivalling that of native mussel proteins, a task that has remained a substantial engineering challenge.

We also find that peptides incorporating the chemically stable amino acid Phe, a functional group that is conspicuously deficient in the sequences of mussel proteins, exhibit reversible adhesion interactions significantly exceeding that of an analogous mussel-mimetic Dopa-containing peptide. The strong reversible cohesion exhibited by the Phe peptide suggests that peptide sequences incorporating Lys and a balance of both Dopa and Phe could provide an attractive approach to develop underwater adhesives, hydrogel-binding groups and other applications that involve peptide cohesion in harsh oxidizing environments.

We conclude that cation–π interactions provide a compelling molecular motif that plays a key role in enabling the robust underwater adhesion exhibited by numerous marine organisms. This picture may provide a molecular basis for understanding the impressive underwater adhesion of marine organisms, such as barnacles[25], that synthesize adhesive proteins lacking the Dopa functional group. More broadly, we demonstrated that interfacial confinement fundamentally alters the energetics of cation–π-mediated assembly, an insight that should prove relevant for diverse areas, from rationalizing biological assembly to engineering peptide-based biomaterials.

Methods

Peptide synthesis and modification. The peptides CGYKGKYYGKGKKYYYK, CGFKGKFFGKGKKFFFK and CGLKGKLLGKGKKLLLK were synthesized by GenScript using routine solid-phase synthesis with N-terminal acetylation and C-terminal amidation and provided as a desalted solid. Mushroom tyrosinase (3,000 U mg^{-1}) was from Aldrich-Sigma. All the reagents were of analytical grade.

Peptide monomers were crosslinked to form dimers. Disulfide linkages provide a facile strategy for the creation of peptide dimers, and additional cysteine residues

could be utilized to create more-complex peptide structures. The monomer (1 mg) was dissolved in 1 ml of 0.1 M phosphate buffer, pH 7.0, and mixed with 10 µl of 5 mg ml^{-1} $NaIO_4$. After shaking for 10 min, the solution was injected into a reverse-phase HPLC using a 260 × 7 mm RP-300 Aquapore column, and eluted with a linear gradient of aqueous acetonitrile. The eluent was monitored continuously at 230 and 280 nm, and 0.33 ml fractions that contained peptides were pooled. Mass spectra of these fractions were obtained on a Micromass QTOF2 tandem mass spectrometer (Waters) with an electrospray ionization source. The fractions that contained pure peptide dimers were collected and freeze dried for future use.

Enzymatic modification to obtain the Dopa peptide. The Tyr peptide (1 mg) was dissolved in 1 ml of 50 mM borate, pH 7.0 and 0.1 M phosphate–ascorbate buffer in an Eppendorf microfuge tube. After adding mushroom tyrosinase (0.3 mg), the tube was shaken for 4 h at room temperature and ambient pressure. Each reaction was stopped by adding 40 µl of glacial acetic acid, and the resulting product was purified with a reverse-phase HPLC column. After being analysed by mass spectrometry, fractions that contained five or six Dopa residues were collected and freeze dried. Each peptide was dissolved in 100 mM acetic acid (Sigma Aldrich) and 250 mM KNO_3 (Sigma Aldrich) buffer (pH 2.5) with a peptide concentration of 1 mg ml^{-1}, and stored at −80 °C.

Intermolecular force–distance ($F(D)$) measurements. $F(D)$ measurements were performed using the protocol in ref. 35. Briefly, peptide-coated mica surfaces were brought into molecular contact in an electrolyte solution of 250 mM KNO_3, 100 mM acetic acid (pH 2.5) at ångström-per-second rates (Figs 2 and 3). After compression, the surfaces were left to equilibrate for at least 5 min and then separated at nanometre-per-second rates, progressively loading the spring, until the surfaces abruptly 'jumped' apart to large separations. This 'jump' distance is used to determine the load on the spring prior to the separation of the two surfaces. This adhesion force is then converted into the work of adhesion, E_{ad}, by using the Johnson–Kendall–Roberts theory of adhesion[11]. Our experimental measurements took place over times that exceeded 24 h and peptide-mediated cohesion was seen to be independent of the measurement time at multiple contact points.

Solid-state NMR measurements. Solid-state NMR measurements were conducted at 11.7 T on a Bruker AVANCE II spectrometer that operated at 500.24 and 125.79 MHz for ^1H and ^{13}C, respectively. Approximately 80 mg of each peptide was packed into a 4 mm zirconia rotor for NMR characterization. Measurements were conducted at 0 °C under conditions of magic-angle spinning (MAS) at 10 kHz using a 4 mm variable-temperature double-resonance Bruker probehead. Magnetization transfer from ^1H to ^{13}C nuclei was achieved by cross-polarization through adiabatic transfer under the Hartman–Hahn condition with a contact time of 1 ms (ref. 48).

The 1D $^{13}C\{^1H\}$ CP-MAS cross-polarization MAS spectra were acquired on the Tyr and Leu samples by signal-averaging 4,096 transients. For the 2D $^{13}C\{^1H\}$ HETCOR spectra, high-power eDUMBO-1_{22} homonuclear decoupling at a radiofrequency field strength of 100 kHz was applied during the evolution period[49]. Scaling factors of 0.65 and 0.63 were calculated for the Tyr and Leu samples from 2D $^{13}C\{^1H\}$ HETCOR spectra of ^{13}C,^{15}N-enriched glycine acquired under identical conditions used for each peptide, applying the constraint that the three ^1H signals in the 2D spectra of ^{13}C,^{15}N-enriched glycine resonate at 3.2, 4.3 and 8.4 ppm. The indirect t_1 dimension for each 2D measurement was incremented by 96 µs, and a total of 60 and 77 t_1 increments was used for the respective Tyr and Leu samples. A total of 1,024 and 512 transients were signal-averaged for each t_1 increment for the Tyr and Leu samples, respectively. Quadrature detection in the indirect (^1H) dimension was achieved by using time-proportional phase incrementation[50]. Heteronuclear ^1H–^{13}C decoupling was achieved by using the SPINAL-64 decoupling sequence with a radiofrequency field strength of 100 kHz (ref. 51). Line broadening of 30 and 10 Hz was applied to the indirect (^1H) and direct (^{13}C) dimensions, respectively. For the 2D spectrum of Tyr, seven contour levels are shown that correspond to 20, 25, 30, 40, 55, 70 and 90% of the maximum signal intensity, whereas for the 2D spectrum of Leu, nine contours are shown that correspond to 3, 5, 7.5, 12, 17, 25, 40, 60 and 90% of the maximum signal intensity. The ^{13}C and ^1H chemical shifts were referenced to tetramethylsilane using tetrakis-methylsilane as an external reference with isotropic ^1H and ^{13}C chemical shifts of 0.25 and 3.52 ppm, respectively[52].

Data availability. Mass spectrometry and HPLC data are available on request.

Received 30 September 2015; accepted 6 December 2015; published online 13 February 2017

References

1. Ma, J. C. & Dougherty, D. A. The cation–π interaction. *Chem. Rev.* **97,** 1303–1324 (1997).
2. Gallivan, J. P. & Dougherty, D. A. Cation–π interactions in structural biology. *Proc. Natl Acad. Sci. USA* **96,** 9459–9464 (1999).
3. Crowley, P. B. & Golovin, A. Cation–π interactions in protein–protein interfaces. *Proteins.* **59,** 231–239 (2005).
4. Madahevi, A. S. & Sastry, G. N. Cation–π interaction: its role and relevance in chemistry, biology, and material science. *Chem. Rev.* **113,** 2100–2138 (2013).
5. Zhong, W. *et al.* From *ab initio* quantum mechanics to molecular neurobiology: a cation–π binding site in the nicotinic receptor. *Proc. Natl Acad. Sci. USA* **95,** 12088–12093 (1998).
6. Khademi, S. *et al.* Mechanism of ammonia transport by Amt/MEP/Rh: structure of AmtB at 1.35 Å. *Science.* **305,** 1587–1594 (2004).
7. Meyer, E. A., Castellano, R. K. & Diederich, F. Interactions with aromatic rings in chemical and biological recognition. *Angew. Chem. Int. Ed.* **42,** 1211–1250 (2003).
8. Hwang, D. S., Zeng, H., Lu, Q., Israelachvili, J. N. & Waite, J. H. Adhesion mechanism in a DOPA-deficient foot protein from green mussels. *Soft Matter* **8,** 5640–5648 (2012).
9. Lu, Q. *et al.* Nanomechanics of cation–π interactions in aqueous solutions. *Angew. Chem.* **125,** 4036–4040 (2013).
10. Kim, S. *et al.* Cation–π interaction in DOPA-deficient mussel adhesive protein mfp-1. *J. Mater. Chem. B* **3,** 738–743 (2015).
11. Israelachvili, J. N. *Intermolecular and Surface Forces* Revised 3rd edn (Academic, 2011).
12. de Gennes, P. G. Soft adhesives. *Langmuir* **12,** 4497–4500 (1996).
13. Rose, S. *et al.* Nanoparticle solutions as adhesives for gels and biological tissues. *Nature* **505,** 382–385 (2014).
14. Sunner, J., Nishizawa, K. & Kebarle, P. Ion–solvent molecule interactions in the gas phase. The potassium ion and benzene. *J. Phys. Chem.* **85,** 1814–1820 (1981).
15. Burley, S. K. & Petsko, G. A. Amino–aromatic interactions in proteins. *FEBS Lett.* **203,** 139–143 (1986).
16. Deakyne, C. A. & Meot-Ner, M. Unconventional hydrogen bonds. 2. NH^+–π complexes of onium ions with olefins and benzene derivatives. *J. Am. Chem. Soc.* **107,** 474–479 (1985).
17. Lee, B. P., Messersmith, P. B., Israelachvili, J. N. & Waite, J. H. Mussel-inspired adhesives and coatings. *Annu. Rev. Mater. Res.* **41,** 99–132 (2011).
18. Wong Po Foo, C. T. S., Lee, J. S., Mulyasasmita, W., Parisi-Amon, A. & Heilshorn, S. C. Two-component protein-engineered physical hydrogels for cell encapsulation. *Proc. Natl Acad. Sci. USA* **106,** 22067–22072 (2009).
19. Norrby, P. & Liljefors, T. Strong decrease of the benzene–ammonium ion interaction upon complexation with a carboxylate anion. *J. Am. Chem. Soc.* **121,** 2303–2306 (1999).
20. Bartoli, S. & Roelens, S. Binding of acetylcholine and tetramethylammonium to a cyclophane receptor: anion's contribution to the cation–π interaction. *J. Am. Chem. Soc.* **124,** 8307–8315 (2002).
21. Hunter, C. A., Low, C. M. R., Rotger, C., Vinter, J. G. & Cristiano, Z. The role of the counterion in the cation–π interaction. *Chem. Commun.* 834–835 (2003).
22. Carrazana-García, J. A., Rodríguez-Otero, J. & Cabaleiro-Lago, E. M. A computational study of anion-modulated cation–π interactions. *J. Phys. Chem. B* **116,** 5860–5871 (2012).
23. Carrazana-García, J. A., Cabaleiro-Lago, E. M., Campo-Caharrón, A. & Rodríguez-Otero, J. A theoretical study of ternary indole-cation-anion complexes. *Org. Biomol. Chem.* **12,** 9145–9156 (2014).
24. Shao, H. & Stewart, R. J. Biomimetic underwater adhesives with environmentally triggered setting mechanisms. *Adv. Mater.* **22,** 729–733 (2010).
25. Kamino, K., Nakano, M. & Kanai, S. Significance of the conformation of building blocks in curing of barnacle underwater adhesive. *FEBS J.* **279,** 1750–1760 (2012).
26. Yamamoto, H. Synthesis and adhesive studies of marine polypeptides. *J. Chem. Soc. Perkin Trans. 1* 613–618 (1987).
27. Yu, M. & Deming, T. J. Synthetic polypeptide mimics of marine adhesives. *Macromolecules* **31,** 4739–4745 (1998).
28. Mattson, K. M. *et al.* A facile synthesis of catechol-functionalized poly(ethylene oxide) block and random copolymers. *J. Polymer Sci. A* **53,** 2685–2692 (2015).
29. Lee, H., Dellatore, S. M., Miller, W. M. & Messersmith, P. B. Mussel-inspired surface chemistry for multifunctional coatings. *Science* **318,** 426–430 (2007).
30. Wang, J. *et al.* Influence of binding-site density in wet bioadhesion. *Adv. Mater.* **20,** 3872–3876 (2008).
31. Wei, W. *et al.* Bridging adhesion of mussel-inspired peptides: role of charge, chain length, and surface type. *Langmuir* **31,** 1105–1112 (2015).
32. Maier, G. P., Rapp, M. V., Waite, J. H., Israelachvili, J. N. & Butler, A. Adaptive synergy between catechol and lysine promotes wet adhesion by surface salt displacement. *Science.* **349,** 628–632 (2015).
33. Danner, E. W., Kan, Y., Hammer, M. U., Israelachvili, J. N. & Waite, J. H. Adhesion of mussel foot protein mefp-5 to mica: an underwater superglue. *Biochemistry* **51,** 6511–6518 (2012).
34. Luckham, P. F. & Klein, J. Forces between mica surfaces bearing adsorbed polyelectrolyte, poly-L-lysine, in aqueous media. *J. Chem. Soc. Faraday Trans. 1* **80,** 865–878 (1984).
35. Israelachvili, J. N. *et al.* Recent advances in the surface forces apparatus (SFA) technique. *Rep. Prog. Phys.* **73,** 036601 (2010).
36. Guo, C. & Holland, G. Investigating lysine adsorption on fumed silica nanoparticles. *J. Phys. Chem. C* **118,** 25792–25801 (2014).
37. De Vita, E. & Frydman, L. Spectral editing in ^{13}C MAS NMR under moderately fast spinning conditions. *J. Magn. Reson.* **148,** 327–337 (2001).

38. Ando, S. *et al*. Conformational characterization of glycine residues incorporated into some homopolypeptides by solid-state ^{13}C NMR spectroscopy. *J. Am. Chem. Soc.* **107,** 7648–7652 (1985).
39. Selection of non-protonated carbon resonances in solid-state nuclear magnetic-resonance. *J. Am. Chem. Soc.* **101,** 5854–5856 (1979).
40. Gomes, J. & Mallion, R. Aromaticity and ring currents. *Chem. Rev.* **101,** 1349–1383 (2001).
41. Sever, M. J., Weisser, J. T., Monahan, J., Srinivasan, S. & Wilker, J. J. Metal-mediated cross-linking in the generation of a marine mussel adhesive. *Angew. Chem. Int. Ed.* **43,** 448–450 (2004).
42. Holten-Andersen, N. *et al*. pH-induced metal–ligand cross-links inspired by mussel yield self-healing polymer networks with near-covalent elastic moduli. *Proc. Natl Acad. Sci. USA* **108,** 2651–2655 (2011).
43. Yu, M., Hwang, J. & Deming, T. J. Role of L-3-4-dihydroxyphenylalanine in mussel adhesive proteins. *J. Am. Chem. Soc.* **121,** 5825–5826 (1999).
44. Lee, H., Scherer, N. F. & Messersmith, P. B. Single-molecule mechanics of mussel adhesion. *Proc. Natl Acad. Sci. USA* **103,** 12999–13003 (2006).
45. Martinez Rodriguez, N. R., Das, S., Kaufman, Y., Israelachvili, J. N. & Waite, J. H. Interfacial pH during mussel adhesive plaque formation. *Biofouling* **31,** 221–227 (2015).
46. Liaqat, F. *et al*. High-performance TiO_2 nanoparticle/DOPA polymer composites. *Macromol. Rapid Commun.* **36,** 1129–1137 (2015).
47. Guardingo, M. *et al*. Bioinspired catechol-terminated self-assembled monolayers with enhanced adhesion properties. *Small* **10,** 1594–1602 (2014).
48. Hediger, S., Meier, B. H., Kurur, N. D., Bodenhausen, G. & Ernst, R. R. NMR cross polarization by adiabatic passage through the Hartmann–Hahn condition (APHH). *Chem. Phys. Lett*. **223,** 283–288 (1994).
49. Elena, B., de Paëpe, G. & Emsley, L. Direct spectral optimisation of proton–proton homonuclear dipolar decoupling in solid-state NMR. *Chem. Phys. Lett*. **398,** 532–538 (2004).
50. Marion, D. & Wüthrich, K. Application of phase sensitive two-dimensional correlated spectroscopy (COSY) for measurements of ^{1}H–^{1}H spin-spin coupling constants in proteins. *Biochem. Biophys. Res. Commun*. **113,** 967–974 (1983).
51. Fung, B. M., Khitrin, A. K. & Ermolaev, K. An improved broadband decoupling sequence for liquid crystals and solids. *J. Magn. Reson.* **142,** 97–101 (2000).
52. Hayashi, S. & Hayamizu, K. Chemical shift standards in high-resolution solid-state NMR (1) ^{13}C, ^{29}Si, and 1H nuclei. *Bull. Chem. Soc. Jpn* **64,** 685–687 (1991).

Acknowledgements

This research was supported by the Materials Research Science and Engineering Centers Program of the National Science Foundation under Award no. DMR 1121053. The authors acknowledge A. Griffin for assistance in characterizing the peptide adsorption.

Author contributions

M.A.G. and W.W. contributed equally to this work. M.A.G., W.W., J.H.W. and J.N.I. conceived the research. M.A.G., A.M.S. and T.R.C. performed and analysed the force–distance measurements, W.W. synthesized and purified the peptides, M.A.G., H.A.D. and M.I. performed the NMR measurements, H.A.D., M.I. and B.F.C. analysed the NMR results, M.A.G. wrote the paper. All of the authors interpreted the data, discussed the results and commented on the manuscript.

Additional information

Supplementary information is available in the online version of the paper. Reprints and permissions information is available online at www.nature.com/reprints. Correspondence and requests for materials should be addressed to J.H.W. and J.N.I.

Competing financial interests

The authors declare no competing financial interests.

nature chemistry

SUPPLEMENTARY INFORMATION

DOI: 10.1038/NCHEM.2720

In the format provided by the authors and unedited.

Tuning underwater adhesion with cation-π interactions

Matthew A. Gebbie, Wei Wei, Alex M. Schrader, Thomas Cristiani, Howard A. Dobbs, Matthew Idso, Bradley F. Chmelka, J. Herbert Waite & Jacob N. Israelachvili

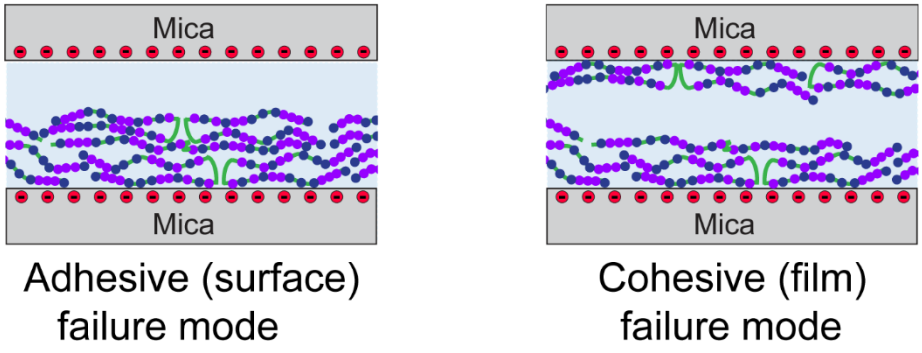

Figure 1. Schematic illustrating the difference between adhesive failure and cohesive failure. In adhesive failure, interactions and/or bonds within films exceed the strength of molecule-surface interactions/bonds, causing the failure plane to be located at the surface-molecule interface. In cohesive failure, solid-molecule interactions/bonds exceed the strength of intermolecular interactions/bonds, causing the failure plane to be located within films. In cohesive failure, the measured work of adhesion is proportional to the strength of intermolecular cohesion. For single molecule adhesives that bridge two surfaces[32], failure necessarily occurs at a molecule-surface interface. In contrast, the peptide films we study fail via a cohesive mode, as discussed in the "Establishing cohesive failure" section below.

Force measurements across symmetric peptide films

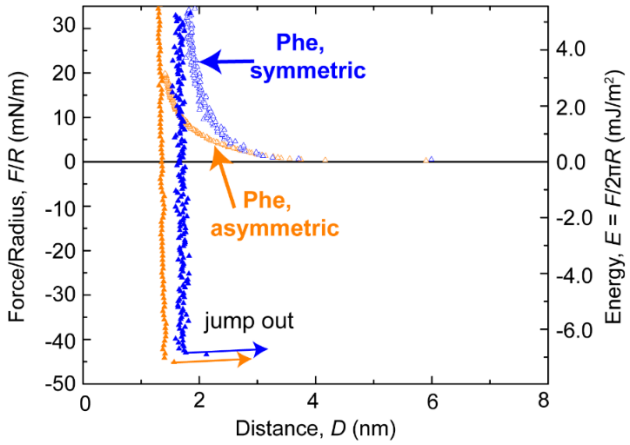

Figure 2. Representative force-distance profiles measured across the highly cohesive Phe peptide, comparing the work of adhesion of peptide films that were deposited onto only one of two mica surfaces (asymmetric, orange) to the work of adhesion of peptide films that were deposited onto both mica surfaces (symmetric, blue).

As discussed in the Methods section of the main text, force-distance measurements across peptide films that are prepared in differing "symmetric" and "asymmetric" experimental protocols provide insight into the failure plane of molecular films. In this work, the adhesion forces measured using both experimental protocols are in quantitative agreement, providing evidence that the failure plane for these Lys- and aromatic rich peptides is located within the peptide film (cohesive failure), as opposed to at the peptide-mica surface. See the "Establishing cohesive failure" section for further discussion.

Table 1. Thickness of peptide films deposited in 100 mM acetic acid, 250 mM KNO_3

Peptide	Asymmetric thickness	Symmetric thickness
Leu	1.6 ± 0.4 nm	2.0 ± 0.4 nm
Phe	1.4 ± 0.6 nm	2.2 ± 0.4 nm
Tyr	2.3 ± 0.6 nm	2 ± 2 nm
Dopa	2.6 ± 0.8 nm	

Salt concentration dependence of adhesion forces

To gain further insight into the mechanism of peptide mediated cohesion, we performed force-distance measurements under differing solution salinities. Specifically, we repeated the cohesion measurements of the Phe peptide and Tyr peptide in constant 100 mM concentrations of acetic acid, with additional background salt concentrations of 0 mM KNO_3 (which is also the deposition salinity), 10 mM KNO_3, 50 mM KNO_3, and 250 mM KNO_3. As shown in Supplementary Figs. 3 and 4, these experiments exhibit the same salt dependence as previous studies of cation-π interactions[9,10].

To make these experiments feasible, we always deposited the peptides under conditions of 100 mM acetic acid with no background KNO_3. We then performed force-distance measurements at KNO_3-free conditions, before sequentially increasing the bulk reservoir salt concentration to 10 mM KNO_3, followed by 50 mM KNO_3, and finally concluding each experiment at 250 mM KNO_3. In all cases, the µL sized SFA fluid reservoir was flushed with >5 mL of solution at each injection step and the surfaces were allowed to sit for 30 min before resuming force-distance measurements to ensure osmotic equilibration.

With this protocol, the Phe peptide exhibits a doubling of cohesion forces when compared to the Tyr peptide for measurements at the deposition salinity, in quantitative agreement with the relative adhesion magnitudes obtained when depositing the peptides under 250 mM KNO_3 conditions. Further, both peptides exhibited a systematic decrease in adhesion forces with increasing salt concentrations, with Phe exhibiting stronger cohesion than Tyr.

Notably, the deposition salinity appears to have a significant impact on the self-assembly of adhesive peptide films. The peptide films that were deposited under KNO_3 free conditions exhibit only a modestly increased adhesion force, compared to films that are deposited under high salt conditions. Further, films that are deposited under salt-free conditions and then sequentially osmotically shocked by increasing the reservoir salt concentration up to 250 mM KNO_3 exhibit a

54 pronounced decrease in adhesion at solution salinity of 250 mM KNO_3, relative to peptide films
55 that are deposited under high salt conditions.

56 Presumably, the deposition salinity impacts the resultant film morphology for these highly
57 charged peptides, and similar effects are observed during the deposition of polyelectrolytes[11].
58 While determining the morphological changes that underlie this observation is beyond the scope
59 of the current study, we conclude that deposition salinity is a critical parameter that needs to be
60 considered when assembling adhesive films. Thus, we hypothesize that the deposition salinity
61 should be approximately matched to the salinity that will be present in applications.

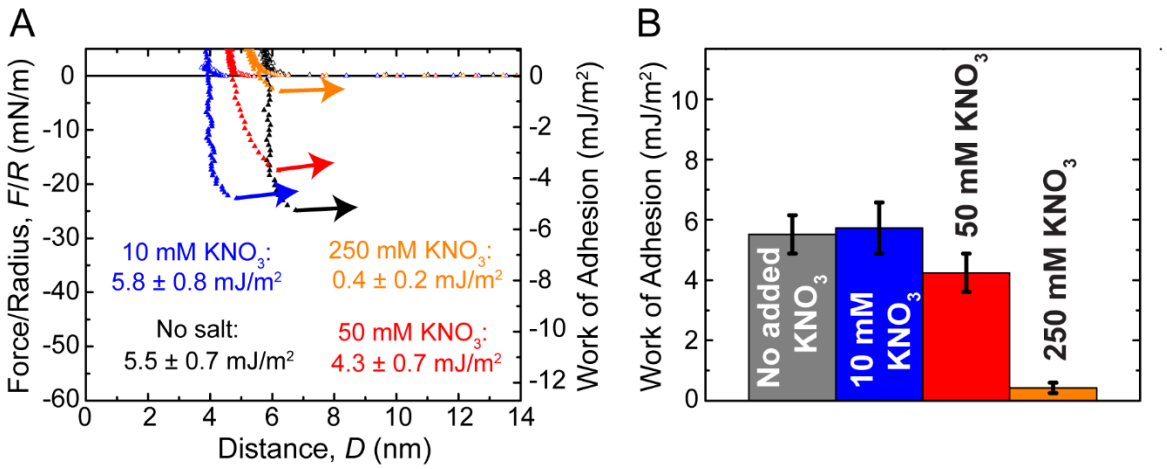

62

63 **Figure 3.** (A) Representative force-distance profiles measured across the Tyr peptide, and (B)
64 bar graph of work of adhesion illustrating the dependence of adhesion forces on solution salinity,
65 with no added KNO_3 (black), 10 mM KNO_3 (blue), 50 mM KNO_3 (red) and 250 mM KNO_3 (orange).
66 In these experiments, peptide films were deposited onto mica surfaces in 100 mM acetic acid
67 buffer with no background KNO_3 electrolyte, and the salinity of the bulk SFA reservoir was
68 incrementally increased from 0 mM KNO_3 to 250 mM KNO_3 through sequential injections of higher
69 salinity solutions.

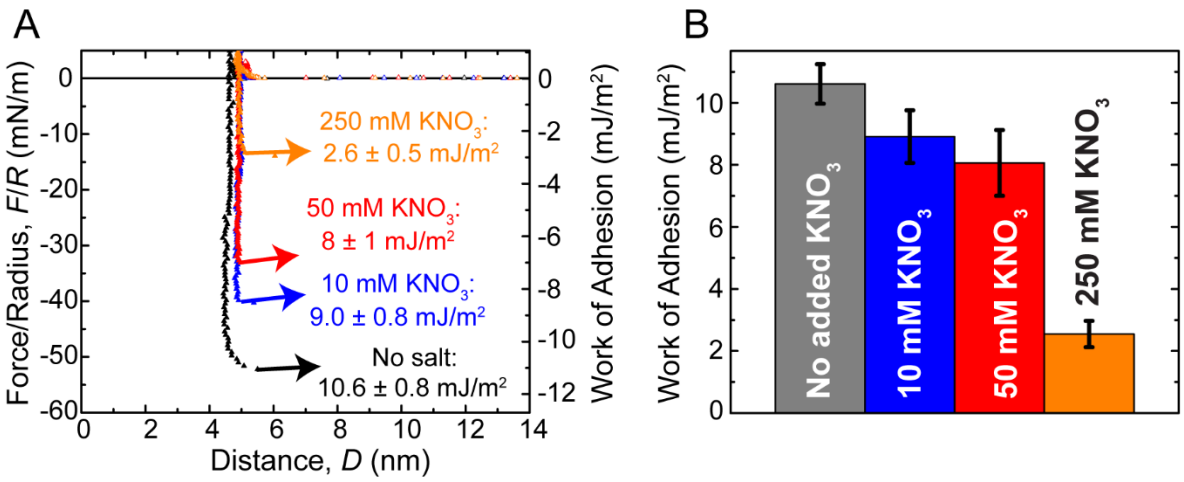

Figure 4. (A) Representative force-distance profiles measured across the highly cohesive Phe peptide, and (B) bar graph of work of adhesion illustrating the dependence of adhesion forces on solution salinity, with no added KNO_3 (black), 10 mM KNO_3 (blue), 50 mM KNO_3 (red) and 250 mM KNO_3 (orange). In these experiments, peptide films were deposited onto mica surfaces in 100 mM acetic acid buffer with no background KNO_3 electrolyte, and the salinity of the bulk SFA reservoir was incrementally increased from 0 mM KNO_3 to 250 mM KNO_3 through sequential injections of higher salinity solutions.

Solid state NMR of Leu peptide

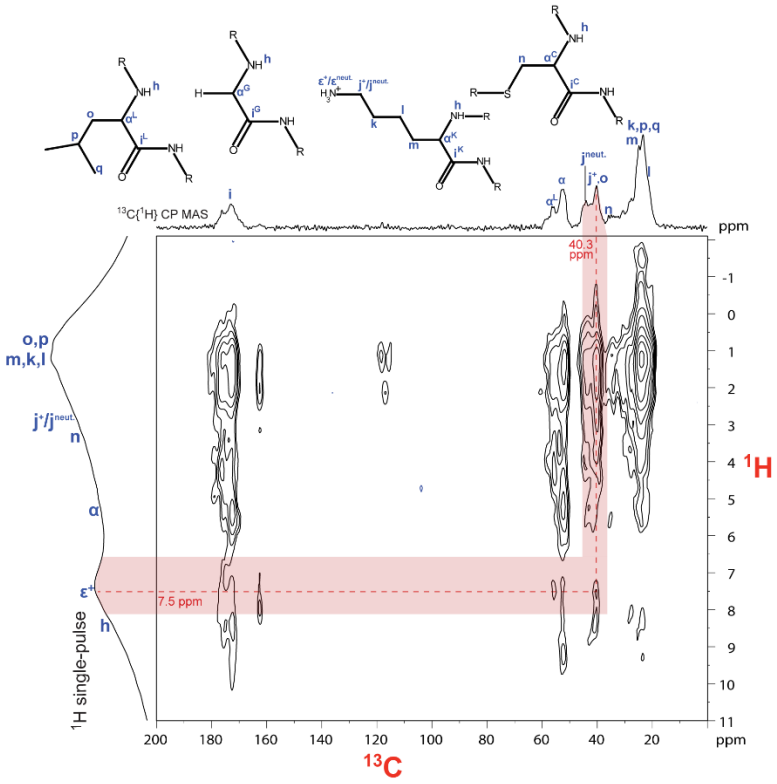

Figure 5. A solid-state 2D ^{13}C{^{1}H} HETCOR MAS NMR spectrum acquired from bulk Leu peptide with a 1D ^{13}C{^{1}H} CP-MAS NMR spectrum shown along the top horizontal axis and single-pulse ^{1}H MAS NMR spectrum along the left vertical axis for comparison. The red dotted lines indicate correlated intensity that arises from the close proximities (<1 nm) of alkyl j^{+} ^{13}C and amide ε^{+} ^{1}H moieties of protonated lysine sidechains, which notably appears at 7.5 ppm in the ^{1}H dimension. By comparison, the intensity correlation from the same alkyl j^{+} ^{13}C and ε^{+} ^{1}H moieties is displaced to lower frequency at 6.9 ppm in the spectrum of Tyr in Figure 1 in the main text, indicating the influences of ring currents associated with cation-π interactions among protonated lysine and tyrosine sidechains. The shaded red bands positioned over the same regions as in Figure 4 in the main text show no correlated intensity at 20-30 ppm, establishing the intensity in this region arises from the close inter-residue proximities of alkyl ^{13}C moieties on lysine and aromatic ^{1}H

moieties of the tyrosine. All NMR measurements were conducted at 11.74 T under 10 kHz MAS conditions at 0°C.

Supplemental Methods

Peptide deposition

Nanoscale films of each peptide were deposited onto freshly-cleaved mica surfaces by immersing the mica surfaces in dilute solutions of peptide for 20 min. For the high salt results reported in the main text, each solution contained a μM concentration of peptide in a background buffer of 250 mM KNO_3 and 100 mM acetic acid (pH 2.5). This protocol enabled reproducible assembly of films of comparable molecular density and thicknesses for each peptide. The thicknesses of the diffusive (~3-5 nm) and compressed (~1-3 nm) peptide films indicates the deposition of multi-layer peptide films onto the mica surfaces (Fig. 2).

For the salt concentration-dependent results, the peptide films were deposited from solutions that contained the same peptide concentration as those reported in the main text, but no background KNO_3. Under these conditions, the deposited diffusive films were of similar thicknesses.

The deposition protocol requires removing the surfaces from the SFA after initially calibrating the thickness of mica surfaces, introducing an uncertainty of up to 2 nm for the thickness of the peptide films. Despite this small systematic error, the film thicknesses do trend with the peptide molecular structure as: Leu ~ Phe < Tyr < Dopa (Fig. 3 and Supplementary Table 1). For each approach and separation measurement, the relative uncertainty between the points in the force-distance profile is below 3 Å, meaning that slope of the compression and the magnitude of the work of adhesion are accurate to Å distance and nN force resolutions.

Establishing cohesive failure

We observe that peptide films deposited on single surfaces can form nanoscale multilayers, even when deposited from dilute solutions. Previously[31], dynamic light scattering

measurements were used to establish that similar short peptide molecules exist as multi-peptide aggregates when dissolved in aqueous solutions and subsequently form nanoscale multilayer films when solution deposited from μM concentration solutions. As a result, we conclude that nanoscale multilayer formation could be a prevalent phenomenon for solution deposited peptide and protein films, and these multilayer films can exhibit cohesive failure modes when confined between two surfaces, even when molecules are deposited on only one of the two surfaces.

Thus, the deposition of peptide or protein on a single surface when testing adhesion forces in nanoscale force measurements is not sufficient to establish that peptide films fail exclusively through adhesive mechanisms; further characterization is required to determine the mechanism of film failure. However, relatively few studies specifically go about distinguishing between cohesive and adhesive failure mechanisms, leaving a fair degree of uncertainty regarding whether previous measurements on the “adhesion” mediated by nanoscale peptide and protein films are probing adhesion or cohesion properties.

A key test of the film failure mechanism is to compare the adhesion of molecular films that are deposited onto only one of the two surfaces to the adhesion of films that are deposited onto both surfaces. In one set of these experiments, peptides were deposited onto a single mica surface and a bare mica surface was used as the second surface for SFA measurements. A second set of experiments was performed where peptides were deposited onto each of the two mica surfaces, creating a symmetric SFA setup. Previously, these two experimental protocols resulted in qualitatively and quantitatively differing force-distance profiles when failure occurs at the protein-surface or peptide-surface interface[17,33]. On the other hand, force-distance experiments that implicated cohesive failure exhibit close agreement for the works of adhesion measured via the two approaches[10,17].

In this work, the measured adhesion forces are in quantitative agreement when the peptides are deposited using both methods (Supplementary Fig. 2). The primary difference between the two experimental protocols is that the compressed peptide films are systematically

thicker when peptide is deposited onto both surfaces, as compared to single surface deposition (Supplementary Table 1). Further, the dominant mechanisms of mica-peptide surface bonding appear to be through the formation of Lys-mica Coulomb bonds and/or peptide backbone hydrogen bonds, interactions that should be independent of the molecular structures of the aromatic amino acids studied. Since alterations to the structure of the aromatic residues result in systematic changes to the measured E_{ad}, we conclude that cohesive failure is the most likely failure mode in these experiments.

Nevertheless, we cannot completely rule out adhesive failure. If these films fail at the mica-peptide interface, then our observation that Phe peptides mediate stronger adhesion than Dopa peptides would be unprecedented, particularly since a recent study of monolayers formed by small aromatic- and Lys- containing molecules at mica surfaces[32] demonstrates that Phe-Lys monolayers exhibit significantly weaker binding to mica surfaces than Dopa-Lys monolayers.

Further, an adhesive mode of failure for these peptide films would imply that intra-film cation-π interactions exceed the strength of electrostatic interactions between Lys- and mica charge sites; however, Lys-mica binding is known to be a strong, specific electrostatic interaction[34]. While such a result would prove to be unexpected and interesting, we find no compelling evidence to support this interpretation.